Nuclear Engineering and Technology 50 (2018) 182–189

Contents lists available at ScienceDirect

Nuclear Engineering and Technology

journal homepage: www.elsevier.com/locate/net

Original Article

Activation analysis of targets and lead in a lead slowing down spectrometer system

Yongdeok Lee [a], Jeong Dong Kim [b], Seong Kyu Ahn [a], Chang Je Park [b, *]

[a] Fuel Cycle Strategy Development Division, Korea Atomic Energy Research Institute, Daedeok-Daero 1045, Yuseong, Daejeon, 305-353, South Korea
[b] Department of Nuclear Engineering, Sejong University, Neungdong-ro 209, Gwangjin-gu, Seoul, South Korea

ARTICLE INFO

Article history:
Received 2 June 2017
Received in revised form
15 October 2017
Accepted 6 November 2017
Available online 24 November 2017

Keywords:
Activation Analysis
CINDER90
Neutron Source
Neutron Slowing Down
Sensitivity

ABSTRACT

A neutron generation system was developed to induce fissile fission in a lead slowing down spectrometer (LSDS) system. The source neutron is one of the key factors for LSDS system work. The LSDS was developed to quantify the isotopic contents of fissile materials in spent nuclear fuel and recycled fuel. The source neutron is produced at a multilayered target by the (e,γ)(γ,n) reaction and slowed down at the lead medium. Activation analysis of the target materials is necessary to estimate the lifetime, durability, and safety of the target system. The CINDER90 code was used for the activation analysis, and it can involve three-dimensional geometry, position dependent neutron flux, and multigroup cross-section libraries. Several sensitivity calculations for a metal target with different geometries, materials, and coolants were done to achieve a high neutron generation rate and a low activation characteristic. Based on the results of the activation analysis, tantalum was chosen as a target material due to its better activation characteristics, and helium gas was suggested as a coolant. In addition, activation in a lead medium was performed. After a distance of 55 cm from the lead surface to the neutron incidence, the neutron intensity dramatically decreased; this result indicates very low activation.

1. Introduction

A high-energy and high-yield neutron production system was designed in an lead slowing down spectrometer (LSDS) system. The source neutron has an important role in the fissile assay of an LSDS system. The source neutron induces fission in fissile materials. Source neutrons are produced at a multilayered target by the bremsstrahlung radiation reaction, namely the (e,γ)(γ,n) reaction. A multilayered target geometry was designed to produce source neutrons effectively and efficiently. The intense source neutrons continuously interact with the target material, structure material, and lead medium. Source neutrons lose their energy in the lead medium [1,2].

LSDS technology is one of the promising nondestructive assay techniques; it enables direct quantitative measurements of the isotopic contents of major fissile materials such as ^{235}U, ^{239}Pu, and ^{241}Pu in spent nuclear fuel or recycled fuel. Many calculations as well as neutron target design to optimize an LSDS system have been conducted for assay accuracy, safety, economics, and reliability of fuel cycle applications, which include pyroprocessing [3–6]. Pyroprocessing produces Pu isotopes and minor actinides for fabrication of fuel used in sodium-cooled fast reactors [7].

For an LSDS system performing fission measurements with proper statistics, commercially available neutron sources, like D-D and D-T, are not sufficient to overcome the background radiation from the spent fuel or recycled material. However, it has been shown that a small and compact linear electron accelerator can generate intense neutrons [1] with a metal plate target. In the designed source neutron system, it was possible to obtain an intensity of 10^{12} n's/sec, with a mean energy of 1 MeV, at a target with an electron energy of 30 MeV and high current electron beam (~600 mA) [8]. The target material is mostly activated. The neutron yields are also affected by the target geometry and the material. Thus, sensitivity simulation for the activation was performed on targets of different materials, geometries, coolants, and lead medium.

CINDER90 [9] was used for the activation analysis of high energy neutrons. CINDER90 can describe space dependent activation based on a three dimensional geometry from MCNP, which includes 3400 nuclides and a 63 group cross-section library, and provides fast neutron (>1 MeV) irradiation capability. Two target materials,

* *Corresponding author.*
E-mail address: parkcj@sejong.ac.kr (C.J. Park).

https://doi.org/10.1016/j.net.2017.11.002

tantalum and tungsten, were considered. For the coolant of the target system, three different gases were considered: air, argon, and helium. Additionally, activation analysis was done for pure lead at different positions in the lead medium.

2. Lumped model for activation analysis

2.1. Conditions for activation analysis

The lumped target geometry was set up as shown in Fig. 1 to examine the status of the activation at each area (target, multiplication, and medium) when a fast neutron is produced. The lump model has a cylindrical shape that is composed of three layers, tantalum, beryllium, and lead, with thicknesses of 2.5, 2.5, and 5 cm, respectively. For actual activation analysis, position dependent neutron fluxes at the target are required and are obtained with the Monte Carlo Code [10]. The information on the neutron flux, specifications of each region, material, irradiation time, and cooling time are the inputs for the CINDER90 code. The irradiation time of the electron beam on the target was assumed to be 10 hour; the electron beam energy was 30 MeV. Seven cooling time steps were chosen at 0.5, 1, and 3 hour, and 1, 7, 30, and 90 days.

In the system, the neutron flux is estimated by the electron intensity, which is generally proportional to the electron beam current. The electron intensity is calculated with Eq. (1):

$$N_E = A \times F \times H \times 6.242 \times 10^{18} \quad (1)$$

where, A is the beam current (mA), F is the pulse width (ns), and H is the frequency (Hz). For the LSDS system, the beam current was about 600 mA, the pulse width was 500 ns, and the frequency was 240 Hz. As a result, the produced electron intensity was 4.5e+14 #/s [11]. Consequently, the generated neutron flux from electrons is calculated simply by multiplying the electron intensity by the neutron production ratio (neutrons per electron) at the target. From the MCNP simulation, the neutron production ratio, 0.01, was used for an incident 30 MeV electron beam.

2.2. Activation analysis

A produced neutron at the target interacts with the target material as well. Neutron capture and decay occurred at the target material and several daughter nuclei were produced. Table 1 shows the major produced nuclei and radioactivity changes with respect to the cooling time for the tantalum target in the lumped model. ^{180}Ta was produced by neutron decay and ^{181}W was produced by beta decay. The radioactivity of the major nuclides was compared during the cooling time of 90 days. From the results, it was found that Hf-181 becomes the major source of activity at 90 days of cooling. After irradiation, ^{180}Ta has the highest intensity; however, it decays quickly after 7 days. It is almost negligible after a sufficient cooling time. However, the ^{181}W nuclide continuously contributes to the activity during the cooling time. The effect of ^{182}Ta is almost negligible during the cooling.

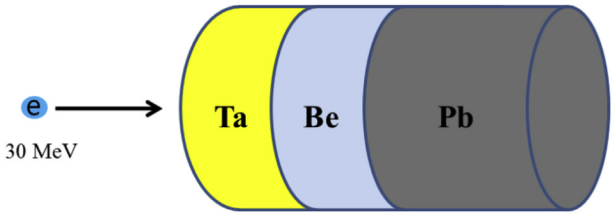

Fig. 1. Geometry of a lumped target.

3. Activation analysis of the target materials

3.1. Target structure and property

From the evaluation of the activation effect using the lumped model, two types of metal target structures were considered for the LSDS system, as shown in Fig. 2, by considering the beam path characteristics. All the layers in the target have cylindrical shapes and consist of tantalum and lead. The type-1 metal target structure consists of five plates each with a different thickness (2, 3, 4, 5, 6 mm) and an identical radius of 7 cm. The type-2 metal target structure also has five plates; however, they have different radii from 3 to 7 cm. The type-1 and type-2 metal target structures have a gap of 1 mm.

The position dependent neutron fluxes at all the target structures were evaluated using the MCNP code. Fig. 3 shows the neutron flux at each layer of the target structure for the type 1 and 2 structures when an electron of 30 MeV is incident. The neutron flux at the type-1 target increases gradually along the electron beam path. The maximum neutron flux occurs on the third plate. However, at the type-2 target, the highest neutron flux is at the first plate and, in contrast, the neutron flux decreases gradually.

Table 2 shows the activation results of the two different types of targets at the maximum neutron flux with respect to the cooling time. The activity of type-1 was much higher than that of type-2 at the beginning. However, when the cooling time increased, the gap in the activity change became smaller than before. Therefore, from the results of the activation analysis, the type-2 structure has a better high neutron generation rate and low activation characteristics.

3.2. Target materials and neutron spectrum

For an effective system using source neutron generation, coolant was also considered in the target design. In addition, a beryllium plate was attached at the end of the target to increase the neutron yield efficiency. Beryllium, because of its low threshold energy for neutron generation, acts as both a neutron reflector and a neutron multiplier in the target system. Fig. 4 shows the target

Table 1
Isotopic activity variation for the lumped target.

Nuclide	Cooling time						
	30 min	1 h	3 h	1 day	7 days	30 days	90 days
	Activity (Ci)						
Hf-181	3.07E-03	3.07E-03	3.07E-03	3.02E-03	2.74E-03	1.88E-03	7.05E-04
Ta-180	1.03E+09	9.85E+08	8.31E+08	1.39E+08	6.70E+02	0.0	0.0
Ta-182	4.38E-07	4.38E-07	2.58E-08	4.35E-07	4.20E-07	3.65E-07	2.54E-07
W-181	2.23E-04	2.23E-04	1.42E-05	2.23E-04	2.14E-04	1.88E-04	1.33E-04
Total	1.03E+09	9.85E+08	8.31E+08	1.39E+08	6.70E+02	2.07E-03	8.38E-04

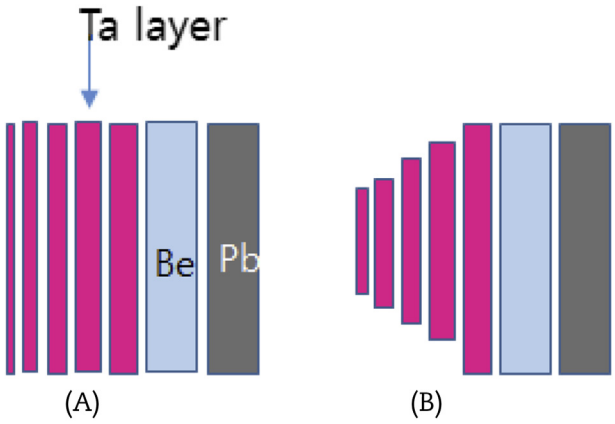

Fig. 2. Configuration of two different target structures. (A) Type-1 target structure. (B) Type-2 target structure.

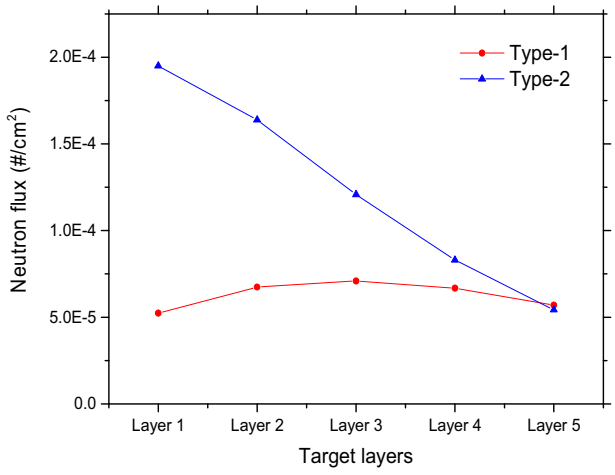

Fig. 3. Neutron fluxes at each layer for two different types of targets.

configuration based on the selected target structure, type-2, which includes a beryllium plate. Two target materials, Ta and W, were considered in the analysis. Tantalum and tungsten are commonly used as target materials for neutron generation. Activation analysis was conducted during the irradiation and cooling time. As shown in Fig. 4, the metal target has a cylindrical shape filled with a noble gas, helium, to prevent the target from melting. The irradiation time was 10 hour and the cooling times were 1 and 3 hour, and 1, 7, 30, 60, and 90 days.

Table 3 shows the total neutron fluxes at each of the Ta and W layers. The neutron flux at the Ta target is slightly higher than that of the W target at the first plate. However, the neutron flux of the W target is higher at the other layers. Fig. 5 shows the neutron energy spectrum of the Ta and W targets. The neutron energy spectra of

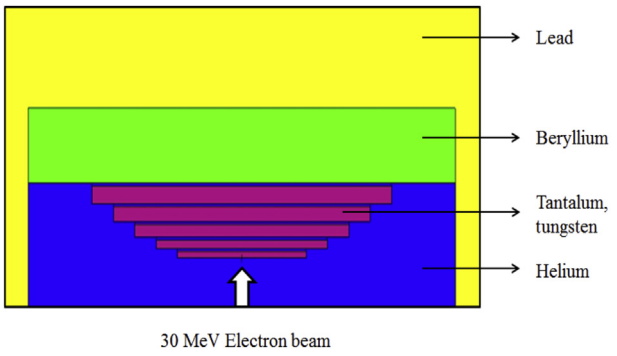

Fig. 4. Proposed metal target geometry for the LSDS system. LSDS, lead slowing down spectrometer.

the Ta and W targets are almost identical. The highest peak at a 1 MeV energy level was obtained at the Ta and W targets; however, the peak at the Ta target is dominant.

3.2.1. Activation analysis during irradiation

The activity change was investigated for the Ta and W targets as a function of the irradiation time. Fig. 6 represents the total activity changes for various irradiation times. The highest activities were obtained at the fifth layer for both the Ta and W targets. For the decided on geometry, when the number of layers increases, the activity increases linearly over the 10 hour irradiation. The total activity of the Ta target decreased gradually as the irradiation time increased. On the other hand, the total activation of the W target was saturated after 1 second of irradiation. However, in the simulation, for 10 hour irradiation, the total activity at the Ta material was significantly larger than that of the W material.

Fig. 7 shows the material inventory change as a function of the irradiation time. The ^{180}Ta nuclide mainly contributes to the total activity of the Ta material; however, it decays quickly during the irradiation time. The daughter nuclides of ^{180}Hf and ^{180}W increase gradually. In the case of the W target, the ^{183}W nuclide mainly contributes to the total activity, and the mass of the major activation products is nearly constant for all irradiation periods. Thus, the activity of the W target is almost constant for the various irradiation times. Table 4 shows the activity according to the different thicknesses after 10 hour of irradiation. The total activity of both the Ta and W targets increases as the thickness increases from 2 to 6 mm. According to the thickness change, the activity rate shows 62%, 51%, 44%, and 38% changes at each step. When going toward the end plate, the activity decreases because the neutrons are captured at the front layers.

3.2.2. Activation analysis during cooling

The activity change was also examined after irradiation, with respect to the cooling time up to 90 days. Table 5 shows the total

Table 2
Activity change for two target geometries at the maximum neutron flux.

Target type	Cooling time						
	30 min	1 h	3 h	1 day	7 days	30 days	90 days
	Activity (Ci)						
Type 1[a]	8.95E+08	8.58E+08	7.24E+08	1.21E+08	5.84E+02	5.35E-04	2.25E-04
Type 2[b]	8.22E+07	7.88E+07	6.64E+07	1.11E+07	5.36E+01	1.53E-04	6.49E-05

[a] 3rd Plateplate.
[b] 1st plate.

Table 3
Total neutron flux incidence at the Ta and W target plates.

Layer of Ta target	Neutron flux (#/cm^{2}s)	FSD[a]	Layer of W target	Neutron flux (#/cm^{2}s)	FSD
Ta1	1.008E+11	0.0761	W1	9.794E+10	0.0743
Ta2	8.082E+10	0.0505	W2	9.300E+10	0.0453
Ta3	6.434E+10	0.0414	W3	7.108E+10	0.0392
Ta4	4.550E+10	0.0354	W4	4.858E+10	0.0331
Ta5	3.178E+10	0.0304	W5	3.353E+10	0.0313

[a] Fractional standard deviation [= relative error=(standard deviation)/(mean)].

activity of the Ta and W targets as a function of the cooling time. After 1 day cooling, the activity of the Ta target is significantly reduced. In the case of the W target, the activity decreases gradually and, at 90 days cooling, the activity is close to that of the Ta activity, at ~10^{-3} Ci.

Tables 6 and 7 provide the material production and major isotopes contributing to total activity for the Ta and W targets after irradiation. For the Ta target, after 7 days, the ^{180}Ta nuclide is totally depleted, and the ^{181}Hf nuclide mainly contributes to the activity. At 90 days, the estimated activity is about 0.001 Ci. For the W target, after 30 days cooling, the ^{187}W nuclide is totally depleted, and only ^{181}W and ^{185}W contribute to the activity. The activity at the W target is approximately 0.001 Ci at 90 days cooling. Therefore, the Ta target has similar activation characteristics to those of the W target for the selected cooling period. However, Fig. 8 shows the total activity change of the targets for 1-year cooling. Before 90 days cooling, the total activity from the Ta target is somewhat higher than that of the W target. After that, the activity at the W target is slightly higher than that of the Ta target because of the different material products. At about 90 days, the major activation products of the Ta target are the ^{181}W and ^{181}Hf nuclides. In case of the W

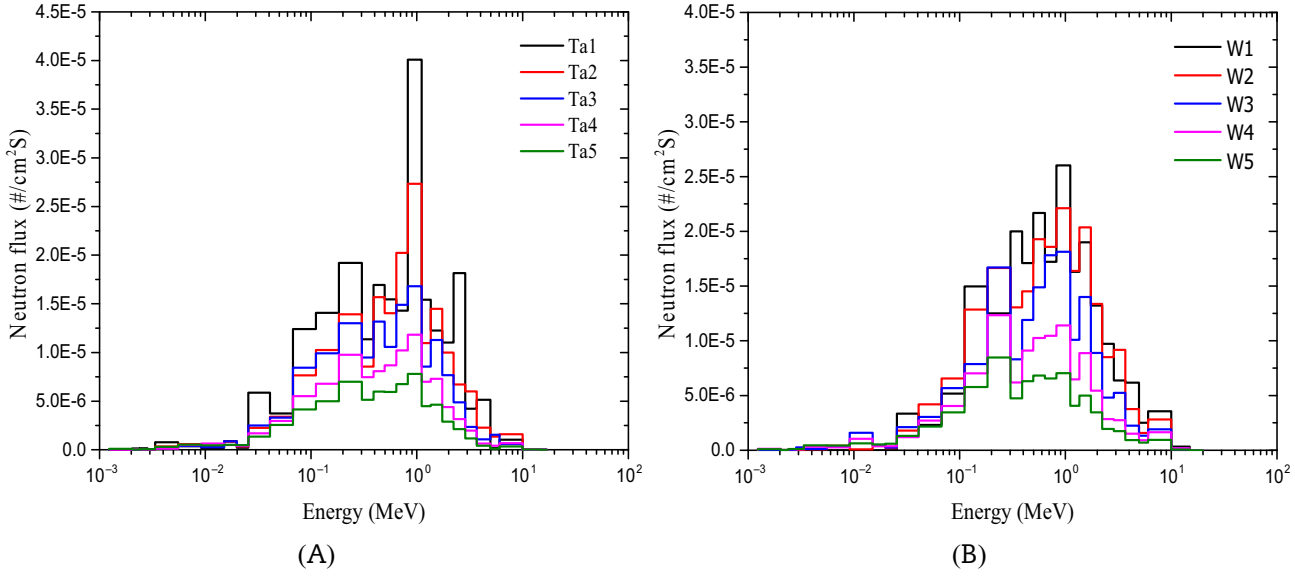

Fig. 5. Neutron energy spectra of Ta and W targets. (A) Ta target. (B) W target.

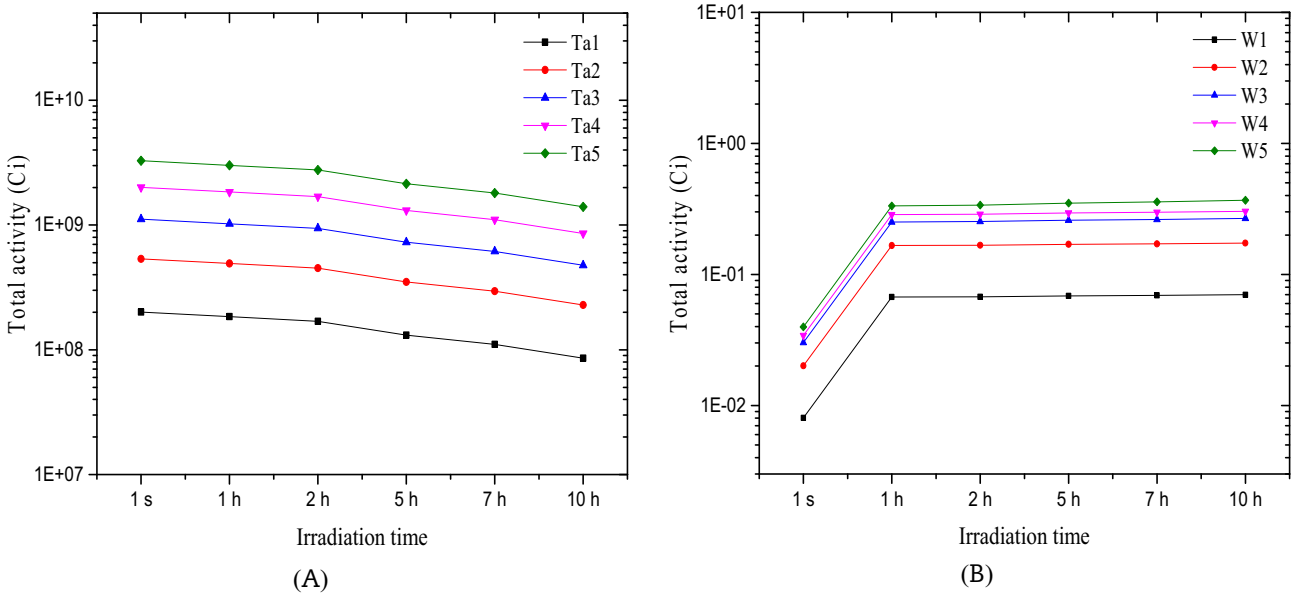

Fig. 6. Total activity changes of Ta and W targets for the irradiation time. (A) Ta target. (B) W target.

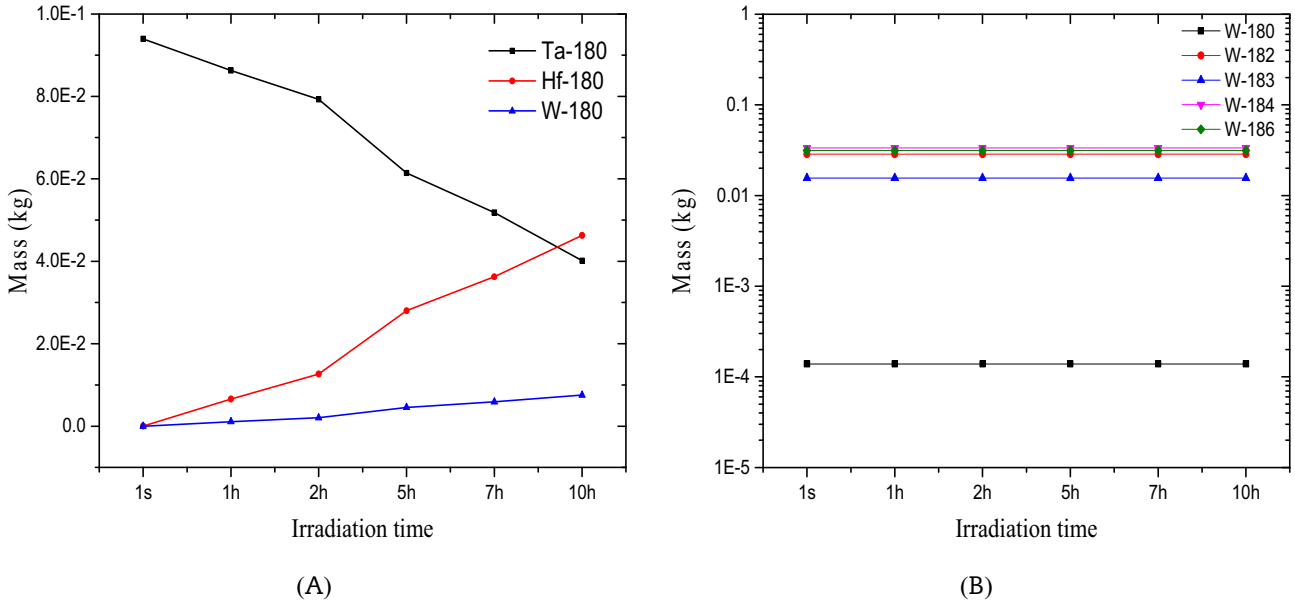

Fig. 7. Material inventory changes of Ta and W targets for the irradiation time. (A) Ta target. (B) W target.

Table 4
Total activity changes for various thicknesses of Ta and W targets.

Total activity (Ci) at 10 h irradiation time					
Thickness	0.2 cm	0.3 cm	0.4 cm	0.5 cm	0.6 cm
Ta	8.58E+07	2.29E+08	4.76E+08	8.58E+08	1.40E+09
W	7.00E-02	1.74E-01	2.68E-01	3.03E-01	3.69E-01

target, the major activation products are the ^{181}W and ^{185}W nuclides. Therefore, for longer cooling, Ta is better for use as a target material.

3.3. Activity change with cooling gases

To generate very intense source neutrons by photonuclear reaction, a high electron energy and current must be incident on the target material. Therefore, the temperature increases beyond the melting point at the target layer. Thus, cooling is a necessary

Table 5
Activities of Ta and W targets as a function of cooling time after a 10 h irradiation.

	Total activity (Ci) for various cooling times							
	1 s	30 min	1 h	3 h	1 day	7 days	60 days	90 days
Ta	3.05E+09	2.92E+09	2.80E+09	2.36E+09	3.96E+08	1.91E+03	1.70E-03	1.11E-03
W	1.24E+00	8.74E-02	8.60E-02	8.10E-02	4.49E-02	2.77E-03	1.35E-03	1.04E-03

Table 6
Contribution of major isotopes to activity in Ta target (%) after irradiation.

Nuclide	Half-life(s)	1 s	30 min	1 h	3 h	1 day	7 days	30 days	60 days	90 days
Hf-179	2.17E+06	0	0	0	0	0	0	0.2	0.1	0.1
Hf-181	3.66E+06	0	0	0	0	0	0	89.9	86.3	81.7
Ta-179	5.74E+07	0	0	0	0	0	0	1.8	2.7	4.1
Ta-180	2.93E+04	100	100	100	100	100	100	0	0	0
W-181	1.05E+07	0	0	0	0	0	0	8.2	10.8	14.1

Table 7
Contribution of major isotopes to activity in W target (%) after irradiation.

Nuclide	Half-life(s)	1 s	30 min	1 h	3 h	1 day	7 days	30 days	60 days	90 days
W-179	2.25.E+03	0.1	0.8	0.5	0.1	0	0	0	0	0
W-181	1.05.E+07	0	0.7	0.7	0.8	1.4	18	23.7	25.7	27.8
W-183	5.20.E+00	91	0	0	0	0	0	0	0	0
W-185	6.49.E+06	0.1	2.5	2.6	2.7	4.9	62.7	76.1	74.2	72.1
W-185	1.00.E+02	3.9	0	0	0	0	0	0	0	0
W-187	8.54.E+04	4.9	95.6	95.9	96.2	93.6	18.9	0	0	0

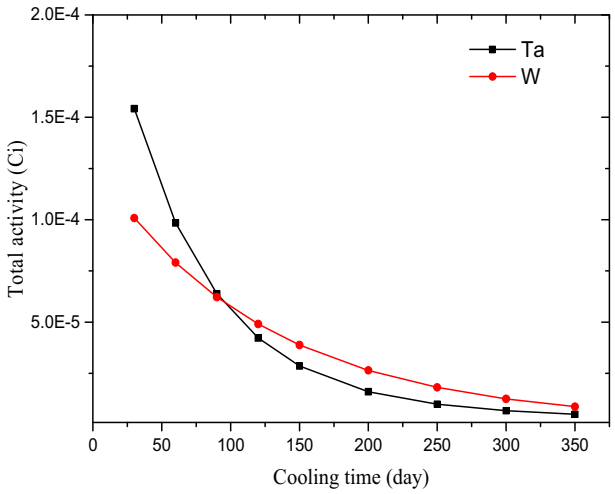

Fig. 8. Total activity changes of Ta and W targets as a function of cooling time up to 350 days.

process at the target to maintain the target temperature below the melting point. The cooling mechanisms can be classified into natural convection and forced circulation. Helium, argon, and air were considered for the cooling gas. Based on the target model shown in Fig. 4, an assessment of the activation analysis was done at up to 90 days for the cooling time with the cooling gas. For the three proposed different cooling gases, the neutron fluxes at each layer of the Ta and W targets were estimated by using the MCNP code; the results are shown in Fig. 9.

In the case of the Ta target, the highest neutron flux appears with the He gas coolant. However, for the W target, a mixed phenomenon was obtained. The activity changes for the different coolants are summarized in Tables 8 and 9. The main difference in the activities for the various cooling gases comes from the different neutron absorption capabilities; however, the absolute differences are insignificant. After 90 days cooling, both the Ta and W targets have similar ranges of activity at about 0.001 Ci, irrespective of the cooling gases.

3.4. Activity change with beryllium reflector

Beryllium (Be) was added next to the target end plate to improve the neutron yield. This is a 2.5 cm thick plate as shown in Fig. 4. Be has the advantage of producing neutrons evenly with relatively low energy bremsstrahlung radiation. Therefore, Be increases the neutron yield effectively at the target end plate. An activation calculation for the beryllium plate was also done with the Ta target. The total activities of beryllium according to the cooling time are summarized in Table 10. The total activities for beryllium are almost constant, at 10^{-7} Ci, which is very low. Therefore, the activation effect in the beryllium reflector is almost negligible.

4. Activation analysis on lead medium

A metal plate target is placed at the center of lead piles in the LSDS system. Neutrons are produced at the center of the lead medium. Produced fast neutrons enter the lead and slow down their energies in the lead by continuous interaction. The full size of the

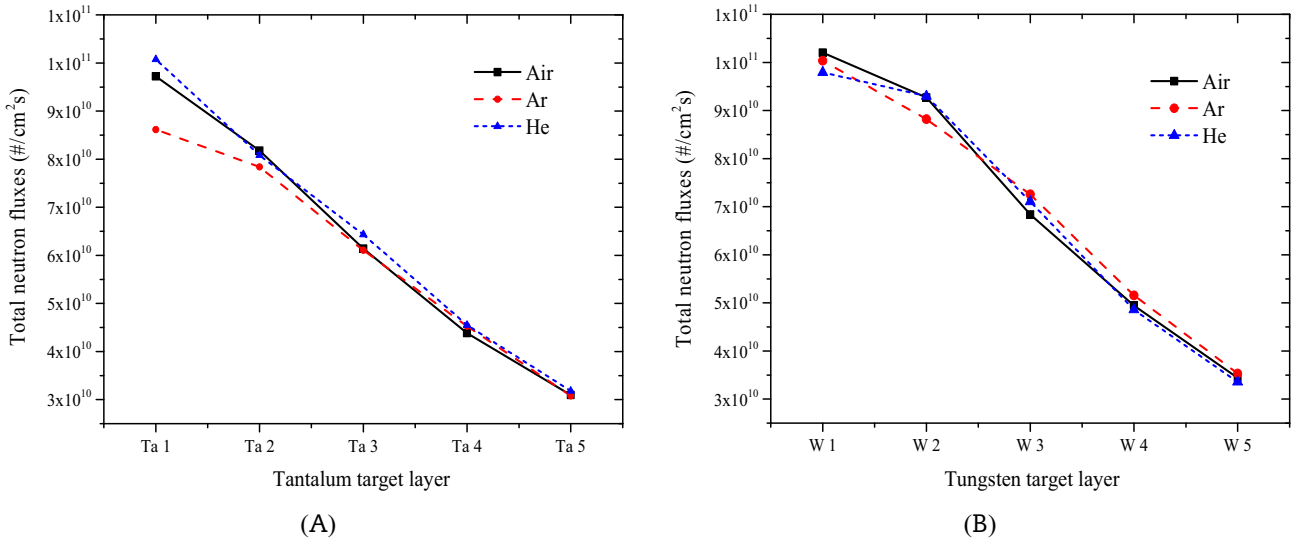

Fig. 9. Neutron fluxes of the Ta and W targets with different cooling gases. (A) Ta target. (B) W target.

Table 8
Total activity changes of the Ta target for various cooling gases.

Cooling gas	Cooling time						
	30 min	1 h	3 h	1 day	7 days	60 days	90 days
Total activity (Ci)							
Argon	2.92E+09	2.80E+09	2.36E+09	3.96E+08	1.91E+03	1.62E-03	1.05E-03
Air	2.92E+09	2.80E+09	2.36E+09	3.96E+08	1.91E+03	1.64E-03	1.07E-03
He	2.92E+09	2.80E+09	2.36E+09	3.96E+08	1.91E+03	1.70E-03	1.11E-03

Table 9
Total activity changes of the W target for various cooling gases.

Cooling gas	Cooling time						
	30 min	1 h	3 h	1 day	7 days	60 days	90 days
Total activity (Ci)							
Argon	7.63E-02	7.50E-02	7.07E-02	3.91E-02	2.38E-03	1.15E-03	8.92E-04
Air	7.19E-02	7.05E-02	6.63E-02	3.69E-02	2.79E-03	1.46E-03	1.14E-03
Helium	8.74E-02	8.60E-02	8.10E-02	4.49E-02	2.77E-03	1.35E-03	1.04E-03

Table 10
Total activity changes of the beryllium reflector for the Ta target.

Material	Cooling time							
	1 s	30 min	1 h	3 h	1 day	7 days	60 days	90 days
Be	Total activity (Ci)							
	1.86E-01	2.05E-07	2.05E-07	2.05E-07	2.05E-07	2.04E-07	2.03E-07	2.02E-07

lead pile is about 170 cm × 170 cm × 170 cm [1]. Fig. 10 shows the simplified activation analysis model for the target system surrounded by lead piles. A total of six lead lumps with different positions were evaluated for the activation analysis. The estimated neutron fluxes and spectra at the different positions in the lead piles are shown in Fig. 11. As the distance from the target grows, the neutron flux dramatically decreases, as shown in Fig. 11.

Tables 11 and 12 summarize the major activation products of the first lead pile, which has the maximum neutron intensity, as shown in Fig. 11, as a function of the irradiation and cooling time.

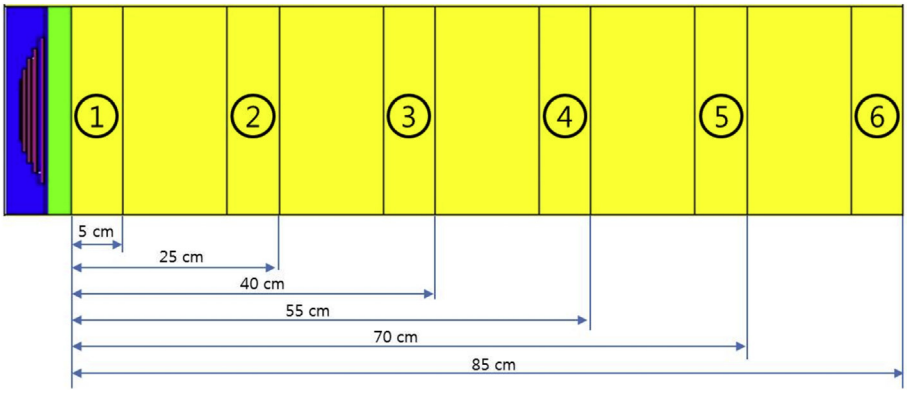

Fig. 10. Simplified activation evaluation position in the lead piles.

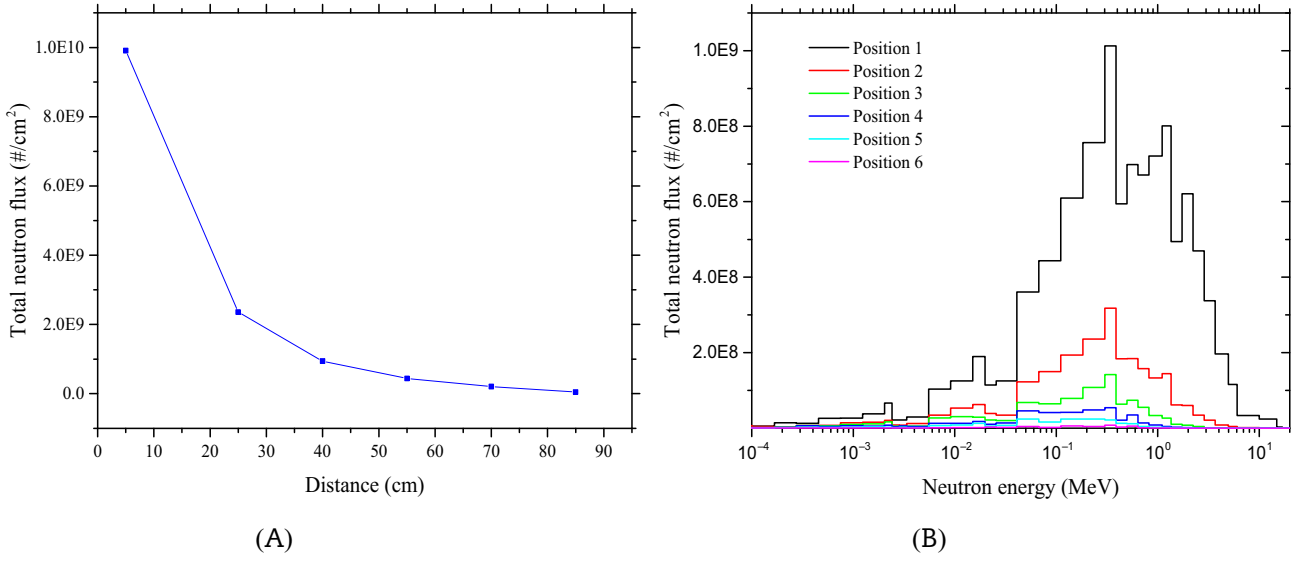

Fig. 11. Neutron fluxes and spectra at different positions in the lead piles. (A) Total neutron flux. (B) Neutron spectrum.

Table 11
Isotopic activities (Ci) of the first lead pile for various irradiation times.

Nuclide	Half-life	Irradiation time					
		1 s	1 h	2 h	5 h	7 h	10 h
H-3	3.89E+08	2.33E-15	8.39E-12	1.68E-11	4.20E-11	5.87E-11	8.39E-11
Hg203	4.03E+06	4.48E-12	1.61E-08	3.22E-08	8.04E-08	1.13E-07	1.61E-07
Pb203	1.87E+05	2.22E-09	1.54E-05	3.05E-05	7.49E-05	1.04E-04	1.45E-04
Pb203m	6.30E+00	6.13E-05	5.88E-04	5.88E-04	5.88E-04	5.88E-04	5.88E-04
Pb204	4.42E+24	3.07E-12	3.07E-12	3.07E-12	3.07E-12	3.07E-12	3.07E-12
Pb204m	4.01E+03	1.65E-06	4.41E-03	6.78E-03	9.10E-03	9.41E-03	9.51E-03
Pb207m	8.05E-01	6.91E-02	1.20E-01	1.20E-01	1.20E-01	1.20E-01	**1.20E-01**
Pb209	1.17E+04	3.69E-07	1.20E-03	2.16E-03	4.08E-03	4.83E-03	5.49E-03

Table 12
Isotopic activities (Ci) of the first lead pile for different cooling times after a 10 h irradiation.

Nuclide	Cooling time						
	1 s	30 min	1 h	3 h	1 day	7 days	90 days
H-3	8.39E-11	8.39E-11	8.39E-11	8.39E-11	8.39E-11	8.38E-11	8.27E-11
Hg203	1.61E-07	1.61E-07	1.61E-07	1.60E-07	1.58E-07	1.45E-07	4.21E-08
Pb203	1.45E-04	1.44E-04	1.43E-04	1.39E-04	1.05E-04	1.54E-05	4.23E-17
Pb203m	5.27E-04	5.77E-90	5.65E-176	0.00E+00	0.00E+00	0.00E+00	0.00E+00
Pb204	3.07E-12	3.07E-12	3.07E-12	3.07E-12	3.07E-12	3.07E-12	3.07E-12
Pb204m	9.51E-03	6.97E-03	5.11E-03	1.47E-03	3.15E-09	4.18E-48	0.00E+00
Pb207m	5.06E-02	0.00E+00	0.00E+00	0.00E+00	0.00E+00	0.00E+00	0.00E+00
Pb209	5.49E-03	4.94E-03	4.44E-03	2.90E-03	3.30E-05	1.56E-18	0.00E+00

Table 13
Total activity changes for different lead pile positions for the Ta target.

Material	Position					
	1	2	3	4	5	6
Lead	Activity (Ci)					
	4.27E-08	4.28E-09	1.69E-11	3.07E-12	3.07E-12	3.07E-12

During the irradiation, the activation of lead is not significant except for metastable products. After 90 days cooling, the activity at the lead becomes very low. ^{203}Hg is the only main active material. Table 13 shows the total activity changes at the different lead pile positions for 90 days cooling. As expected, the activity decreases as the lead piles increase. However, the total activity is very low and is negligible during the operation of the lead slowing down spectrometer.

5. Conclusion

Activation analysis was used to examine the target geometry and materials, the additional beryllium plate, the cooling gas, and the lead medium. The analysis is necessary for system management and safe operations. Information on material activation is also necessary to estimate the lifetime and durability for utilization. For an actual description of material interaction of fast neutrons with the target material and lead medium, the position dependent neutron flux and the energy spectrum were used in the CINDER90 code. Usually, low activation characteristics are preferable for the structural material and cooling gas of the target. Based on the results of the various calculations, a different radius target structure is a good choice; Ta is a good candidate material for the target, due to the relatively short half-life of its activation products. As a coolant, among normal gases such as argon and air, helium gas provides good performance. It has better cooling capacity. In addition, it was found that the activation of the beryllium is almost negligible and yields a lead pile with very low activation.

Conflicts of interest

All contributing authors declare no conflicts of interest.

Acknowledgments

This work was supported by the Nuclear Research Foundation of Korea (NRF) grant funded by the Korea government (MSIP) (No. 2017M2A8A5015084).

References

[1] Y.D. Lee, C.J. Park, H.D. Kim, K.C. Song, Design of LSDS for isotopic fissile assay in spent fuel, Nucl. Eng. Technol 45 (2013) 921–928.
[2] Y.D. Lee, C.J. Park, S.J. Ahn, H.D. Kim, Development of lead slowing down spectrometer for isotopic fissile assay, Nucl. Eng. Technol. 46 (2014) 837–846.
[3] Y.D. Lee, N.M. Abdurrahman, R.C. Block, Design of a spent-fuel assay device using a lead spectrometer, Nucl. Sci. Eng. 131 (1999) 45–61.
[4] H.R. Radulescu, N.M. Abdurrahman, A.I. Hawari, B.W. Wehring, Pulsed neutron Generator Facility for Slowing Down Time Spectrometry, ANRCP-1999-29, 1999.
[5] D. Rochman, R.C. Haight, J.M. O'Donnel, A. Michaudon, S.A. Wender, D.J. Vieira, E.M. Bond, T.A. Bredeweg, A. Kronenberg, J.B. Wilhelmy, T. Ethvignot, T. Granier, M. Petit, Y. Danon, Characteristics of a lead slowing-down spectrometer coupled to the LANSCE accelerator, Nucl. Instrum. Met. Phy. Res. A 550 (2005) 397–413.
[6] C.J. Park, M.K. Jaradat, L. Alawneh, Y.D. Lee, Metal plate target design for the lead slowing down time spectrometer (LSDTS), Ann. Nucl. Energy 49 (2012) 218–222.
[7] K.C. Song, H.S. Lee, J.M. Hur, J.G. Kim, D.H. Ahn, Y.Z. Cho, Status of pyroprocessing technology development in Korea, Nucl. Eng. Technol 42 (2010) 131–144.
[8] S.J. Ahn, J.D. Kim, Y.G. Kim, Y.D. Lee, C.J. Park, Neutron Source Design for Lead Slowing Down Time Spectrometer, ANPU2014, Jeju, Korea, 2014. Nov 9-12, 2014.
[9] W.B. Wilson, S.T. Cowell, T.R. England, A.C. Hayers, P. Moller, A Manual for CINDER'90 Version 07.4 Codes and Data, Los Alamos National Laboratory report, 2008. LA-UR-07-8412, 2008.
[10] D.B. Pelowitz, MCNPX User's Manual, LA-CP-07–1473, Los Alamos National Laboratory, 2008.
[11] J.D. Kim, Y.D. Lee, H.S. Kang, Optimization of operation parameters of 80-keV electron gun, Nucl. Eng. Technol 47 (2014) 387–394.